Article:
Chintalwad, S., Krishnamurthy, S., Ramakrishna, B. et al. (2 more authors) (2020) Investigation of QED Effects with Varying Z in Thin Foil Targets. IEEE transactions on plasma science. 9212612. pp. 573-577. ISSN 1939-9375

https://doi.org/10.1109/TPS.2020.3026781

143

Investigation of QED effects with varying Z in thin foils

S Chintalwad, S Krishnamurthy, B Ramakrishna
Department of Physics, Indian Institute of Technology Hyderabad, India.
S Morris, C Ridgers
Department of Physics, University of York, UK.

Abstract — Quantum electrodynamics (QED) effects in intense laser plasma interaction were investigated using Particle in Cell (PIC) simulations, specifically the generation of electron-positron pairs. Linearly polarized intense laser pulses were used to irradiate a thin foil (1 µm) with an intensity of 4×10^{23} Wcm^{-2}. A scan of targets with varying Z (Al, Cu and Au) is investigated to determine the effect of target Z/density on electron-positron pair production. The total number of pairs created for Al and Cu targets is 10^{14} and 10^{13} respectively. In the case of Au, we did not observe any pair production to occur. We have also calculated the variation in electron energy in these targets. The results indicate that target Z plays a very important role with the laser interaction in the pair production process, which will be explained in this paper.

Email: bhuvan@iith.ac.in

***Index Terms*— Electron-positron pair, Laser-plasma interaction, PIC simulation, QED effects.**

I. Introduction

Strickland and Mourou invented the chirped pulse amplification (CPA) technique, which has led to a dramatic enhancement of laser intensities in excess of 10^{18} Wcm^{-2}**[1].** The physics that emerges when such extremely powerful, short-duration electromagnetic pulses produced by a modern cutting-edge laser system interact with solid-density matter is of fundamental importance for the high power (multi-petawatt) laser installations that might be opened up by future developments in both laser and laser-based technology. The focused laser intensity around 10^{21}Wcm^{-2} is now routinely accessible, whereas intensities greater than 10^{22} Wcm^{-2} will be accessible on target soon. At intensities above 10^{23} Wcm^{-2} quantum electrodynamics (QED) effects start to play a role in interactions of the laser pulse with matter [2-5]. When such intense laser pulse interacts with thin foils, relativistic plasma is produced and this enables us to explore the quantum-dominated regime of laser interaction with matter. Experimentally, pair production caused by high intensity lasers was first observed in 1997, at the Stanford Linear Accelerator Centre (SLAC). It was realized through a collision of a 46.6 GeV electron beam with a laser beam of 1.3×10^{18} Wcm^{-2}. The high energy photon was first produced via nonlinear Compton scattering of electron beams with laser, and then the electron-positron pairs were created via the multiphoton Breit-Wheeler process in which high energy photons collide with the incoming laser [6-10].

QED cascade is possible if multiple generations of electron-positron pairs are created by the laser fields. This happens when the electrons and positrons produced by Breit-Wheeler process radiate high-energy photons by non-linear Compton scattering which further decays into new pairs and so on. The QED cascade effects from two counter-propagating laser pulses and the dependency of cascade rate on intensity and polarization of the laser are reported by Grismayer et al [18]. Similar study by Luo et al [19] gives an estimate of the QED cascade saturation. Based on a semi-analytical scaling for the pair plasma density and corresponding PIC simulations, the dependency of QED cascade on initial target density has been presented by Slade-Lowther et al [20]. In fact, they have also shown that there exist three different cascade regimes with respect to initial target density in high intensity laser-thin foil interaction. In this paper, we use particle-in-cell (PIC) code EPOCH, to perform the simulation studies with QED effects included in the code. Two essential strong-field QED emission processes (i.e., emission of high-energy photons via Compton scattering in the very nonlinear, synchrotron-like regime and multi-photon Breit-Wheeler pair production) are included in the code. Such QED-PIC code has already been used to demonstrate the dominant generation of γ-rays and electron-positron pairs in high intensity laser-matter interaction [11,12,13]. In our case, two-dimensional EPOCH simulations are performed to investigate and compare the generation of dense electron positron plasma and emission of γ-ray from thin foil targets irradiated by a single laser pulse. We investigated three targets with different Z i.e. (Al, Cu and Au) having thickness of 1µm for QED effects.

II. QED-Processes

The high-energy photon produced from non-linear inverse Compton scattering is given by $e^- + n\gamma_l \rightarrow e^- + \gamma_h$ and the electron-positron pair produced by Breit-Wheeler process are represented by $\gamma_h + n\gamma_l \rightarrow e^- + e^+$ where γ_l and γ_h are laser photon and high energy photon respectively [14,15]. Non-linear (QED) effects are determined by the dimensionless parameters η and χ. The parameter η broadly gives the importance of nonlinear Compton scattering by the electrons and χ determines the rate of pair production from these high-energy photons. η is given by,

$$\eta = \left(\frac{\Upsilon}{E_s}\right)|E_\perp + \beta \times cB|$$

where Υ is the Lorentz factor of the emitted electron or positron and E_s is the Schwinger field

$$E_s = \frac{m_e c^2}{|e|\lambda\!\!\!^{-}_c} = 1.3 \times 10^{18} V m^{-1}$$

where m_e, c, e, B and $\lambda\!\!\!^{-}_c$ are mass of electron, speed of light in vacuum ,electron charge, magnetic field and Compton wavelength respectively. χ is given by,

$$\chi = \frac{\hbar\omega \left| E_\perp + \left(\frac{ck}{k}\right) \times B \right|}{2 m_e c^2 E_s}$$

where $\hbar\omega$ is γ-ray photon energy, k is wave vector and $\hbar k$ is photon momentum. $E_\perp$is electric field perpendicular to the motion of electron or positron. If η approaches unity the probability of pair creation increases dramatically[9]. QED routines are incorporated in the PIC code EPOCH. The model in the QED-PIC code EPOCH and inclusion of Monte-Carlo algorithm for calculating the emission of gamma rays and pairs in strong laser fields is described in much greater detail in [16].

III. Simulation Setup

P-polarized laser with a wavelength of 1μm is focused to a spot with radius 1μm leading to peak intensity of about 4×10^{23} Wcm^{-2}. The laser pulse incorporated in the simulation has a square temporal profile with a pulse duration of 30fs. The simulation box sizes are taken to be $10\lambda_l \times 10\lambda_l$ where λ_l is the wavelength of the incident laser. Target is a fully ionized (Al/Au/Cu) foil with thickness of 1μm discretized on a spatial grid with cell size 10nm and the foil is represented by 1000 macro-electrons and 32 macro-ions per cell.

IV. Simulation Results and Discussions

The electron density distribution is shown in Fig.1 for each target. These snapshots are taken at 50fs. The maximum electron density is observed with the Au, whereas Cu has a lower electron density compared to Au and Al has the lowest electron density among the three targets. When a high intense laser pulse interacts with a foil target the ponderomotive force of the pulse evacuates the electrons in that region and therefore leads the electrons to acquire transverse momentum. This process of evacuation of electrons in the region of laser incidence leads to hole-boring. An interesting difference between each of the targets here is that, the high density bunches (red bunches in the density profile) created about the laser incidence region are separated by a significant distance in Al compared to that of Cu which is an indication of early onset of the hole boring process in Al compared to Cu. Au appears to have no onset of hole boring. This difference in the onset of hole boring is due to the difference in electron densities in the three targets.

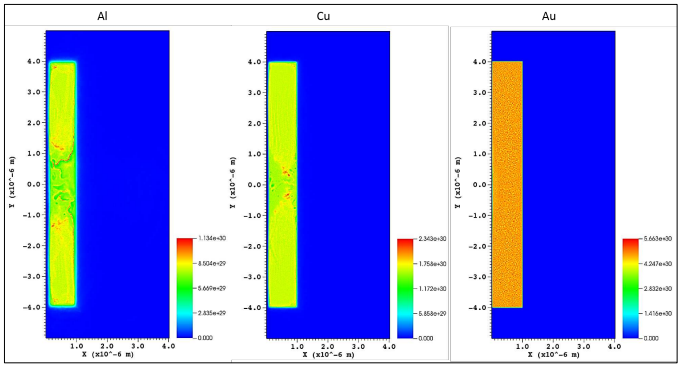

Fig. 1. Snapshot of Electron number density (m^{-3}) obtained at 50fs

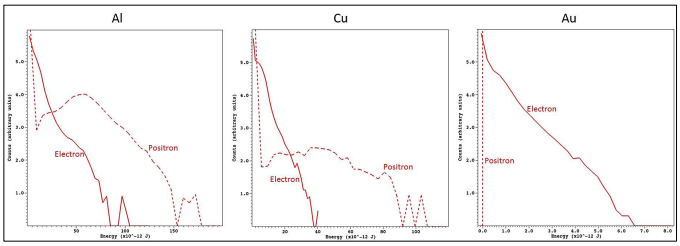

Fig. 2a. Energy spectra of positron and electron

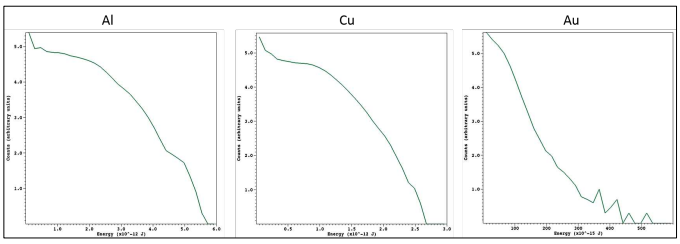

Fig. 2b. Energy spectra of gamma ray.

The electron, positron energy spectra and gamma ray energy spectra for all the three targets are shown in the Fig.2a and 2b respectively. The maximum energy of electron for Al, Cu and Au is 656 *MeV* (105×10^{-12}J), 244 *MeV* (39×10^{-12}J) and 41 *MeV* (6.5×10^{-12}J) respectively. For positron the energy is found to be 1112 *MeV* (178×10^{-12}J) ,669 *MeV* (107×10^{-12}J) and 0 *MeV* (0J) respectively. The observations from the simulation suggest that the positrons have higher energy than the electrons in all three targets. The enhancement in the positron energy arises because the positrons gets accelerated from the sheath field which adds up to the total energy of the positrons. The contribution of sheath field in enhancement of positron energy has been experimentally verified by reducing the magnitude of the sheath electric field by increasing the scale length on the rear side of the target [22]. This is achieved by irradiating the rear side of the target by a ns pulse. Reduction in the sheath field has resulted in reduction in the maximum energy observed for the positrons. The maximum γ-ray energy observed is 36 *MeV* (5.7×10^{-12}J), 16 *MeV* (2.53×10^{-12}J) and 3 *MeV* (0.53×10^{-12}J) for Al, Cu and Au target respectively. From the comparison between positron and corresponding γ-ray energy spectra for all the three targets, it is noted that the positron energy is much higher compared to the γ-ray energy which implies that the positrons once produced by the γ-ray gets rapidly accelerated by the laser field and hence acquires higher energy. There are no positrons observed in case of Au as the corresponding γ-ray energy is very low compared to other two targets.

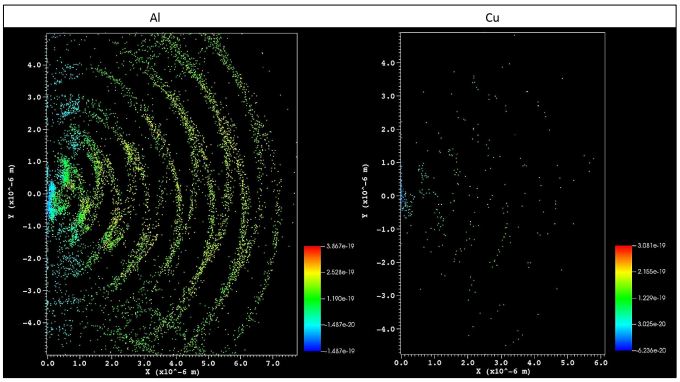

Fig. 3a. Positron phase-space distribution with momentum in units of kgms^{-1}

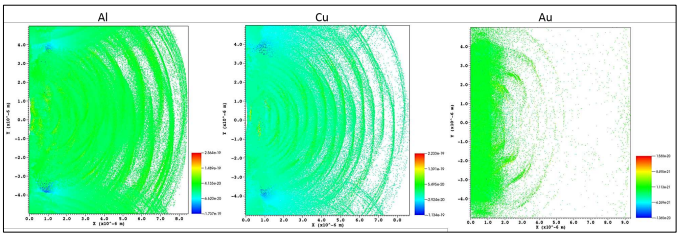

Fig. 3b. Electron phase-space distribution with momentum in units of kgms^{-1}

Fig.3a. shows phase-space distribution of positrons at 30fs in Al and Cu. Phase space distribution for Au is not included in the figure as there are no positrons observed for Au. Among Al and Cu target there is a significant difference in the phase-space distribution which appears to be a consequence of lower flux of positrons in Cu compared to Al.

Fig.3b. shows phase-space distribution of electrons at 30fs in all three targets. It is evident that electrons with momentum along the target normal is abundant in case of Al and Cu compared to Au.

The comparison between each target with respect to the corresponding number of positrons and electrons created is presented in the below Fig.4.

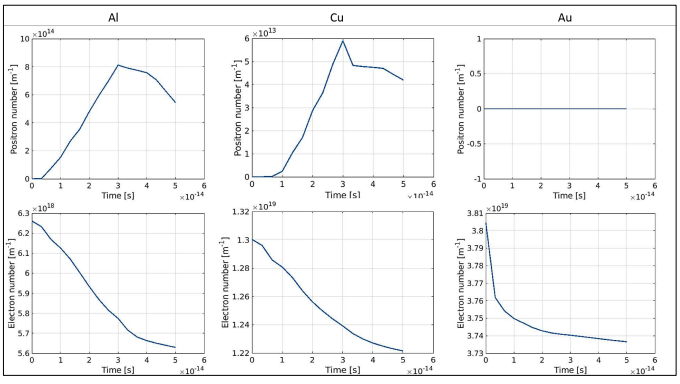

Fig. 4. Positron and electron number

The particle-id feature included in the EPOCH code is used to track and count the number of particles like positrons, electrons or photons created in the interaction. We use a simple MATLAB script to extract the information on the number of particles produced in the simulation. From the above figure it is observed that at 30fs there are 8×10^{14} positrons created in Al, 6×10^{13} positrons created in Cu and no positrons created in Au target and the corresponding number of electrons at 30fs are around 5.76×10^{18}, 1.24×10^{19} and 3.74×10^{19} for Al, Cu and Au respectively. Though the total number of electrons is highest in case of Au, the number of high energy electrons which are travelling along the target normal is comparatively low. Therefore, the primary process of non-linear inverse Compton scattering is significantly reduced leading to lower number of γ-ray photons in Au. In support of this observation, Fig.5 below shows γ-ray energy distribution corresponding for all the three targets.

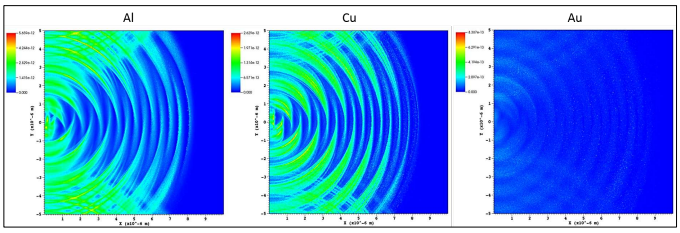

Fig. 5. Gamma-ray spatial distribution with energy in units of J

The observations depict that the γ-ray flux for Al is higher than that for Cu and the lowest flux is observed for Au. These observations are consistent with the corresponding positron number observed for each target (Fig. 4.).

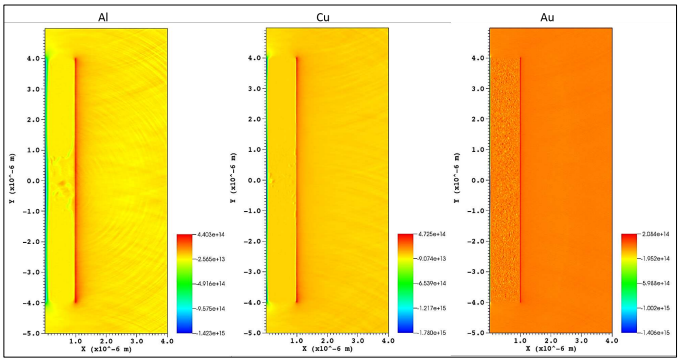

Fig. 6. Snapshot of Electric field (Vm^{-1}) along the direction of laser propagation.

Positrons are created at the region of laser irradiation where the target ionizes and the sheath electric field on the rear side of the target accelerates the positrons rapidly and thereby follows the laser field as shown in Fig.6. Positrons are also expected to follow the same trend as their dynamics depend on the laser field parameters. The positron phase space distribution shown in Fig.3a. infers that our observations are in line with the expected distribution. The electric field strength and magnetic field strength are observed to be strongest in case of Al among the three targets and therefore the corresponding positron flux is also the highest for Al.

From the results of simulation, it is clear that the electron density which depends on the Z of the target plays a very important role in the onset of QED-effects [21]. The physical interplay between QED-effects and the target Z can be understood by considering the laser skin depth inside the target. Longer the laser penetration depth inside the target, higher will be the number of electrons that interact with the laser field. Therefore, Plasma skin depth

$$l_s = \frac{c}{\left(56 \times 10^3 \sqrt{N_e}\right)}$$

where c is the speed of light and N_e is electron density is calculated for all three targets and it is found to be 6nm, 3.8nm and 2.4nm for Al, Cu and Au respectively. Since the skin depth for Al is found to be the highest among the three, QED-effects are dominant in Al whereas the QED-effects are suppressed in Au as it has the least skin depth among the three targets. In addition to this, the value of η calculated from the simulations above are found to be 0.42 and 0.32 for Al and Cu targets respectively. Whereas, in case of Au the value of η is around 0.012, which is very low compared to Al and Cu. Therefore, pair production is not observed in Au.

Our studies above are supported by the work done by Ridgers et al [17]. But in our case we have used different simulation set-up and we have observed the dependence of QED-effects on the Z of the target by using three different targets Al, Cu and Au. The table below summarizes observed parameters and the comparison between each target.

Quantity	Al	Cu	Au
Max. Electron number density.	1.13 ×$10^{30}$$m^{-3}$	2.34×$10^{30}$$m^{-3}$	5.66×$10^{30}$$m^{-3}$
Avg. Electron number density.	5.6×10^{28} m^{-3}	1.2×10^{29} m^{-3}	3.7×10^{29} m^{-3}
Max. Electron energy.	656 MeV	244 MeV	41 MeV
Max. Positron energy.	1112 MeV	669 MeV	0 MeV
Max. Photon energy.	36 MeV	16 MeV	3 MeV
Number of pairs created.	8 × 10^{14}	6 ×10^{13}	0
Number of photons created.	1.8 × 10^{19}	1.06 × 10^{19}	1.1 × 10^{18}
Max. Electric field.	4.4×10^{14} Vm^{-1}	4.7×10^{14} Vm^{-1}	2.1×10^{14} Vm^{-1}

Simulations have also been performed for all the three targets by changing the thickness so that they have the same areal density 6.02×$10^{22}$$m^{-2}$. Fig.7 below shows the corresponding positron and electron numbers.

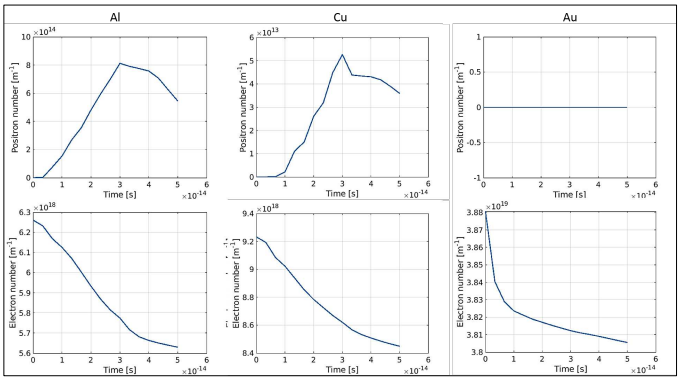

Fig. 7. Positron and electron number for all three targets having same areal density.

For the configuration with same areal density it is observed that at 30fs there are 8×10^{14} positrons created in Al, 5.3×10^{13} positrons created in Cu and no positrons created in Au target and the corresponding number of electrons at 30fs are around 5.76×10^{18}, 8.62×10^{18} and 3.81×10^{19} for Al, Cu and Au respectively. The energy spectrum is shown in Fig.8.

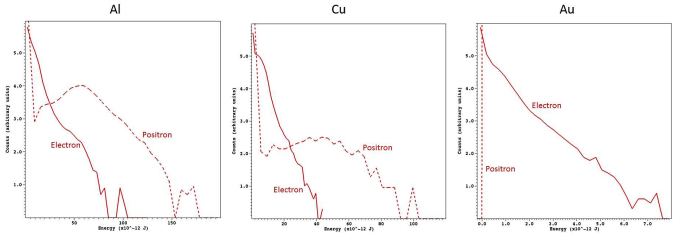

Fig. 8. Positron and electron energy spectra for all three targets having same areal density.

The maximum energy of electron for Al, Cu and Au is 656 *MeV* (105×10^{-12}J), 262 *MeV* (42×10^{-12}J) and 47.5 *MeV* (7.6×10^{-12}J) respectively. For positrons the energy is found to be 1112 *MeV* (178×10^{-12}J) ,650 *MeV* (104×10^{-12}J) and 0 *MeV* (0J) respectively. By comparing the results of Figs.2 and 4 with Figs. 7 and 8 (same areal density) we conclude that the physical trend remains exactly the same.

V. CONCLUSIONS

In conclusion, we have performed PIC simulations using EPOCH to understand the QED effects arising from the interaction of a 10PW laser pulse with thin foils of different Z. The observations mainly include the electron-positron pairs creation via multi-photon Breit-Wheeler process and emission of γ-ray photons via non-linear Compton scattering process. Our observations infer that higher the atomic number of the target, lower the number of pairs created and the γ-ray photons because of the lower skin depth of the laser pulse for higher atomic number targets. Lower skin depth implies lesser interaction between the laser pulse and the target. Therefore, the

QED-effects are dominant in Al than in Cu and Au. Similar effects have been observed from targets with same areal density.

References

[1] A. D. Strickland and G. Mourou, "Compression of amplified chirped optical pulses," Opt. Commun. 56, 219 (1985).
[2] V.Yanovsky et al. Opt Express 16, 2109 (2008).
[3] G.Mourou, T. Tajima, S. V. Bulanov, Rev. Mod. Phys. 78, 309 (2006).
[4] M. Marklund, P.K. Shukla, Rev. Mod. Phys. 78, 591 (2006).
[5] A. Di Piazza, C. Muller, K. Z. Hatsagortsyan, C. H. Keitel, Rev. Mod. Phys. 84, 1177 (2012).
[6] D.L. Burke, R.C. Field, G. Horton-Smith, J.E. Spencer, D. Walz, et al., Positron production in multiphoton light-by-light scattering, Phys. Rev. Lett. 79 (1997) 1626e1629.
[7] C. Bamber, S.J. Boege, T. Koffas, T. Kotseroglou, A.C. Melissinos, et al., Studies of nonlinear QED in collisions of 46.6 GeV electrons with intense laser pulses, Phys. Rev. D 60 (1999) 092004.
[8] L.V. Keldysh, Ionization in the field of a strong electromagnetic wave,Sov. Phys. JETP 20 (1965).
[9] Bell A R and Kirk J G 2008 Possibility of Prolific Pair production with High-Power Lasers, Phys. Rev. Lett. 101 200403.
[10] Kirk J G, Bell A R and Arka I 2009 Pair production in counter-propagating laser beams Plasma Physics and Controlled Fusion 51 085008.
[11] C. P. Ridgers, J. G. Kirk, R. Duclous, T. G.Blackburn, C. S. Brady, K.Bennett, T. D. Arber, and A. R. Bell, J. Comput. Phys. 260, 273–285(2014).
[12] T. Erber, Rev. Mod. Phys. 38, 626 (1966).
[13] V. I. Ritus, J. Russ. Laser Res. 6, 497 (1985).
[14] A. Di Piazza, K. Z. Hatsagortsyan, and C. H. Keitel, Phys. Rev. Lett. 105, 220403 (2010).
[15] D. L. Burke, R. C. Field, G. Horton-Smith, J. E. Spencer, D. Walz, S. C.Berridge, W. M. Bugg, K. Shmakov, A. W. Weidemann, C. Bula, K. T. McDonald, E. J. Prebys, C. Bamber, S. J. Boege, T. Koffas, T.Kotseroglou, A. C. Melissinos, D. D. Meyerhofer, D. A. Reis, and W.Ragg, Phys. Rev. Lett. 79, 1626 (1997).
[16] C. P. Ridgers, C. S. Brady, R. Duclous, J. G. Kirk, K. Bennett, T. D. Arber, and A. R. Bell, Phys. Plasmas 20, 056701 (2013).
[17] C. P.Ridgers, C. S. Brady, R. Duclous, J. G. Kirk, K. Bennett, T. D. Arber, A. P. L. Robinson, and A. R. Bell, Phys. Rev. Lett. 108, 165006 (2012).
[18] T. Grismayer, M. Vranic, J. L. Martins, R. A. Fonseca and L. O. Silva, Phys. Plasmas 23, 056706 (2016).
[19] Luo. W, Liu. W, Yuan. T, et al., QED cascade saturation in extreme high fields. Sci Rep 8, 8400 (2018).
[20] C. Slade-Lowther, D. Del Sorbo, C. P. Ridgers, New J. Phys. 21 013028 2019.
[21] C. S. Brady, C. P. Ridgers, T. D. Arber, A. R. Bell, arXiv:1312.5313
[22] Hui Chen, S. C. Wilks, D. D. Meyerhofer, et al., Phys. Rev. Lett. 105, 015003.